ACS OMEGA

http://pubs.acs.org/journal/acsodf

Article

Structure–Property Relationship of Geopolymers for Aqueous Pb Removal

Sukanta K. Mondal, Adam Welz, Fateme Rezaei, Aditya Kumar, and Monday U. Okoronkwo*

Cite This: https://dx.doi.org/10.1021/acsomega.0c02591

Read Online

ACCESS | Metrics & More | Article Recommendations

ABSTRACT: The geopolymer—an inorganic polymeric material synthesized from the reaction of aluminosilicate precursors and alkaline activating solutions—has gained wide research attention in recent decades as a promising adsorbent for the removal of aqueous heavy metals. However, the high variability of the material and several unanswered questions have limited its development and general adoption in the industry. This study evaluates the impacts of composition and microstructure on the performance of geopolymers for aqueous lead (Pb) removal to elucidate the composition–structure–property relationship. The Pb sorption kinetics and efficiency of four geopolymers, prepared using different fly ash precursors and activating solutions, were investigated. Although all the four geopolymer compositions studied displayed a high Pb removal efficiency of over 99.5%, with a slight decrease in efficiency with increasing Ca/(Si + Al) and Al/Si contents, the results show that the sorption kinetics decreases exponentially with increasing Ca/(Si + Al) and Al/Si molar ratios. The performance of the geopolymers also shows strong correlation to the microstructure, wherein the sorption kinetics increases exponentially, while the efficiency increases slightly, with increasing mass fraction of the amorphous phase in the geopolymer's phase assemblage. The results of this research indicate that using appropriate precursor formulation and curing conditions to evoke the best microstructures, geopolymer materials can be optimized for high performance in removing heavy metals, thereby improving the chances of the material's general acceptability in the adsorbent industry.

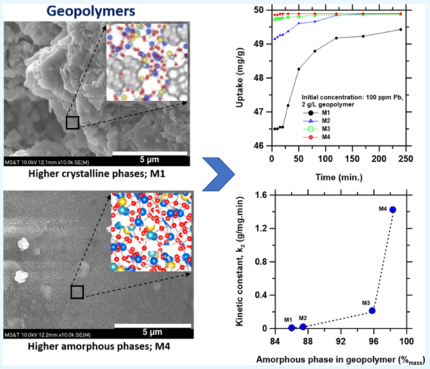

1. INTRODUCTION

The growing industrial and other anthropogenic activities in the world have led to increase in the discharge of effluents containing a high amount of heavy metals into the environment and freshwater resources.[1] Such contamination of freshwater is a significant health concern as heavy metals cannot be broken down to nontoxic forms and, therefore, have enduring adverse effects on the ecosystem.[2] As a result, over 1.2 billion people worldwide do not have access to safe portable water, leading to various health issues and the death of about 14,000 people daily.[3] Lead (Pb) is one of the most hazardous heavy metal pollutants discharged into the environment through various industrial processes such as petroleum refining, lead-containing pesticides, waste batteries, and paints.[4−6] The accumulation of Pb in the body (i.e., lead poisoning) can affect virtually every organ system in the body—it can damage the central nervous system organs (e.g., the brain), digestive system organs (e.g., kidney and liver), and the reproductive system.[6−8] At high concentration levels, Pb can cause coma, convulsions, and death (especially in children).[9,10]

A significant number of methods have been studied to remove such heavy metals from aqueous solution, for example, chemical precipitation, ion exchange, ultrafiltration, reverse osmosis, electrodialysis, and adsorption.[1,11−13] Among these methods, adsorption is remarkably efficient[14,15] and provides opportunity for cost reduction through the use of "suitable" inexpensive natural and waste adsorbents.[16−18] The geopolymer[19−21]—a material prepared from the widely and abundantly available fly ash aluminosilicate material—is a promising eco- and cost-efficient adsorbent for heavy metal sorption.[22−28] It has been particularly shown to perform well for the removal of cationic metals (e.g., Pb).[29] Owing to its chemical characteristics and three-dimensional structure,[20,30] the geopolymer is capable of removing and immobilizing heavy metal ions through a combination of physicochemical, electrostatic, and sorption mechanisms.[26,31−38] It is also known to be stable in a wide range of pH and can be made reusable with appropriate material design.[39]

Despite the unique properties and potentials of geopolymers, the material is yet to gain general acceptance into the mainstream of adsorbents for water and wastewater treatment. This is due to the high degree of variability of this material which

Received: June 1, 2020
Accepted: August 10, 2020

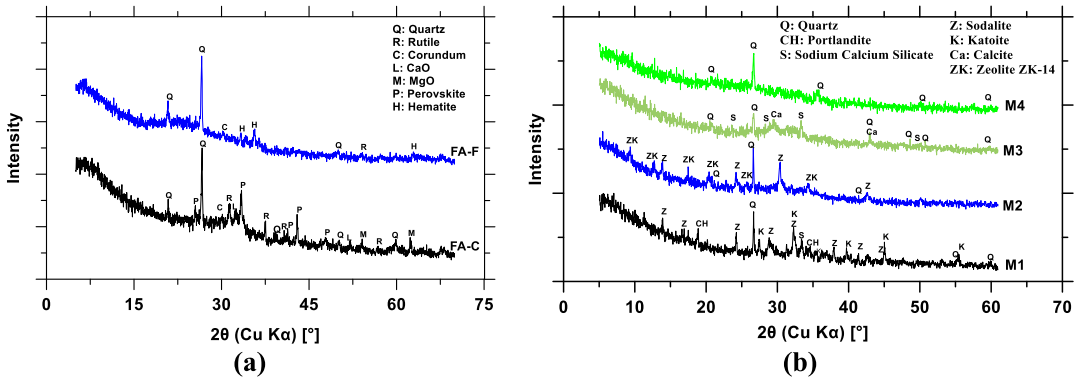

Figure 1. XRD patterns of (a) fly ash precursors; (b) synthesized geopolymers. M1 = geopolymer prepared with FA-C and NaOH; M2 = geopolymer prepared with FA-F and NaOH; M3 = geopolymer prepared with FA-C and Na_2SiO_3; M4 = geopolymer prepared with FA-F and Na_2SiO_3. The corresponding Joint Committee on Powder Diffraction Standards (JCPDS) powder diffraction file numbers of the identified phases are quartz (085-0335), hematite (073-0603), perovskite (42-0423), rutile (21-1276), corundum (074-1081), lime (078-0649), magnesia (077-2364), sodalite (015-0734), zeolite ZK-14 (084-0699), portlandite (04-0733), calcite (086-2339), sodium calcium silicate (012-0670), and katoite (077-1713).

Table 1. Quantitative XRD of Geopolymers and Fly Ash Samples

	crystalline phases ($\%_{mass}$)								
sample[a]	quartz	portlandite	sodium calcium silicate	katoite	sodalite	zeolite, ZK-14	calcite	total	amorphous phases ($\%_{mass}$)
M1	0.9	4.5	1.5	7.1				14.0	86.0
M2	1.5				1.7	9.4		12.6	87.4
M3	2.5	0.6					1.0	4.2	95.8
M4	1.7							1.7	98.3
FA-C								23.5	76.5
FA-F								8.1	91.9

[a]FA-C = type C fly ash; FA-F = type F fly ash; M1 = geopolymer prepared with FA-C and NaOH; M2 = geopolymer prepared with FA-F and NaOH; M3 = geopolymer prepared with FA-C and Na_2SiO_3; M4 = geopolymer prepared with FA-F and Na_2SiO_3.

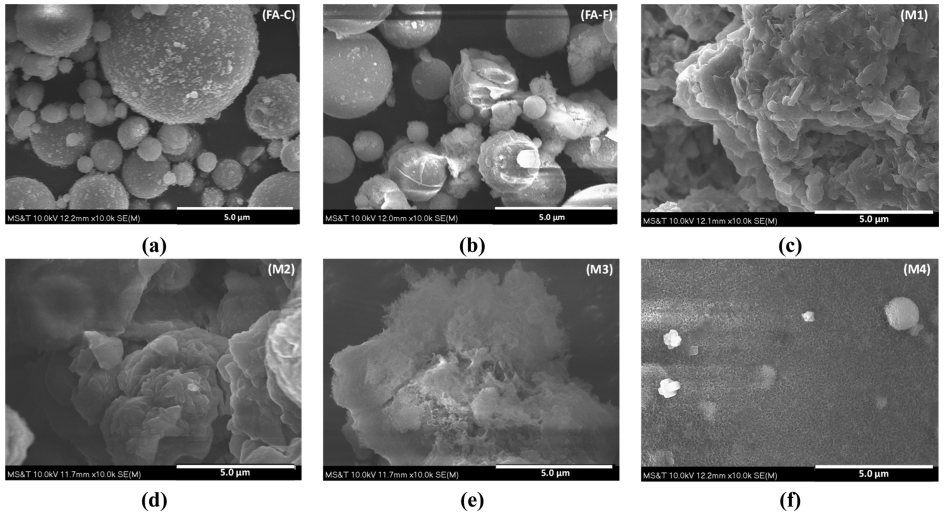

Figure 2. SEM images of fly ash and synthesized geopolymer samples: (a) class C fly ash (FA-C), (b) class F fly ash (FA-F), (c) geopolymer prepared with FA-C and NaOH (M1), (d) geopolymer prepared with FA-F and NaOH (M2), (e) geopolymer prepared with FA-C and Na_2SiO_3 (M3), and (f) geopolymer prepared with FA-F and Na_2SiO_3 (M4). Bright spots are due to charging, suggesting insufficiency of the gold coating.

is derived from aluminosilicate precursors that vary widely in composition and properties globally, for example, fly ash and clay, and the lack of thorough studies on the impact of the variable composition on the heavy metal sorption performance. Most of the available research work on the effect of composition often focuses on geopolymers for structural applications.[20] Hence, this paper presents the first study to examine the composition−structure−property relationships of geopolymers for aqueous Pb removal. Special emphasis was placed to correlate the Pb sorption kinetics and efficiency with the geopolymer composition and microstructure.

2. RESULTS AND DISCUSSION

2.1. Geopolymer Characterization. The X-ray diffraction (XRD) patterns of the fly ash precursors and synthesized geopolymers are shown in Figure 1, and the result of the quantitative XRD analysis is presented in Table 1. The major crystalline phases observed in the fly ashes include quartz,

https://dx.doi.org/10.1021/acsomega.0c02591
ACS Omega XXXX, XXX, XXX−XXX

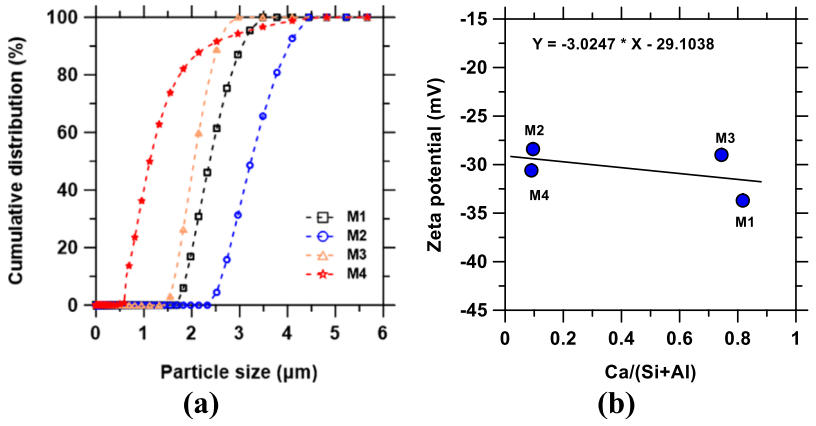

Figure 3. (a) Particle size distribution of pulverized geopolymer samples used for adsorption studies; (b) zeta potential of the geopolymer particles dispersed in deionized water vs the Ca/(Si + Al) ratio of geopolymer composition. Broken lines are "visual guides".

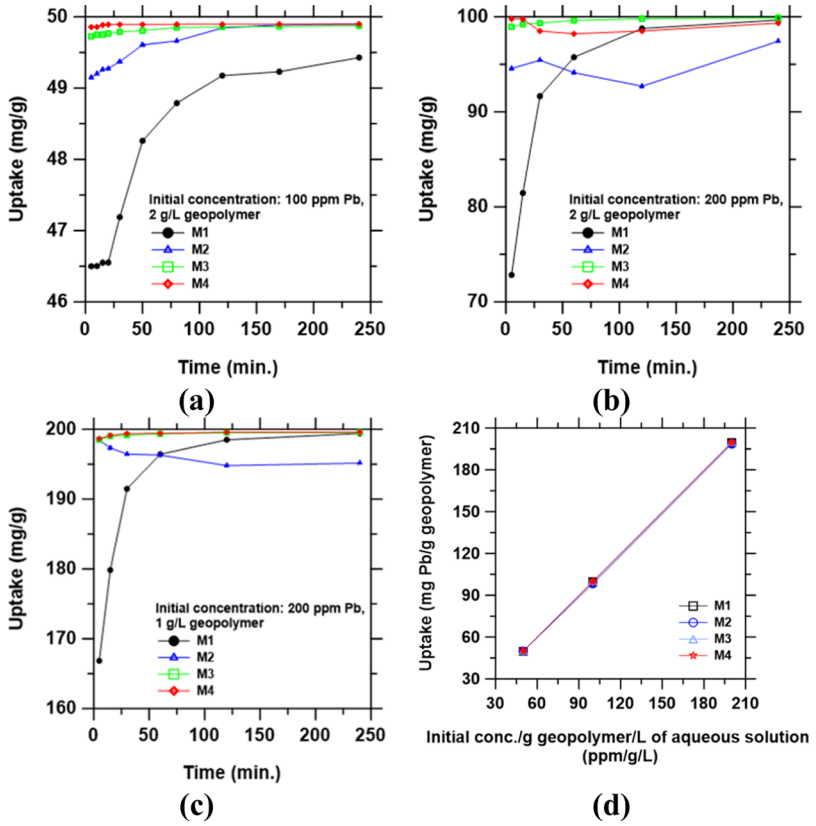

Figure 4. Pb uptake as a function of time for the different sorption setups with initial Pb concentrations and geopolymer dosages of (a) 100 ppm and 2 g/L, (b) 200 ppm and 2 g/L, and (c) 200 ppm and 1 g/L, respectively, and (d) uptake as a function of initial Pb concentration per adsorbent dosage. The lines are "visual guides".

hematite, perovskite ($CaTiO_3$), and rutile, wherein the glass content (i.e., the reactive amorphous phases) represents 76.5 and 91.9% of the type C fly ash (FA-C) and type F fly ash (FA-F), respectively. As seen in Figure 1b, after geopolymerization, most of the crystalline phases in the fly ash (e.g., corundum, lime, and magnesia) and the glass contents reacted to form the amorphous geopolymer (with new minor crystalline phases, e.g., sodalite, zeolite ZK, portlandite, and katoite forming in addition, Figure 1b). Given the differences in the composition of the precursor fly ashes and the chosen activating solutions, some of the synthesized materials are more a "geopolymer-like" alkali-activated material than the pure geopolymer, for example, the high-Ca systems that are composed of a significant amount of crystalline phases may also contain amorphous components that would mainly correspond to a geopolymer-like calcium-(sodium)-alumina-silicate-hydrate (C(N)-A-S-H) gel, and the sodium silicate-activated materials may feature a low degree of fly ash reaction, but for simplicity, all synthesized adsorbents in this study are referred to as geopolymers.[20]

The scanning electron microscopy (SEM) images are displayed in Figure 2, showing the smooth spherical fly ash particles (Figure 2a,b) which had transformed into different morphologies in M1 to M4 (Figure 2c–f) after the alkali activation and hydration. The morphological structures of fly ash and geopolymer samples are found similar to the published articles.[40,41] The geopolymers that were prepared with NaOH

https://dx.doi.org/10.1021/acsomega.0c02591
ACS Omega XXXX, XXX, XXX−XXX

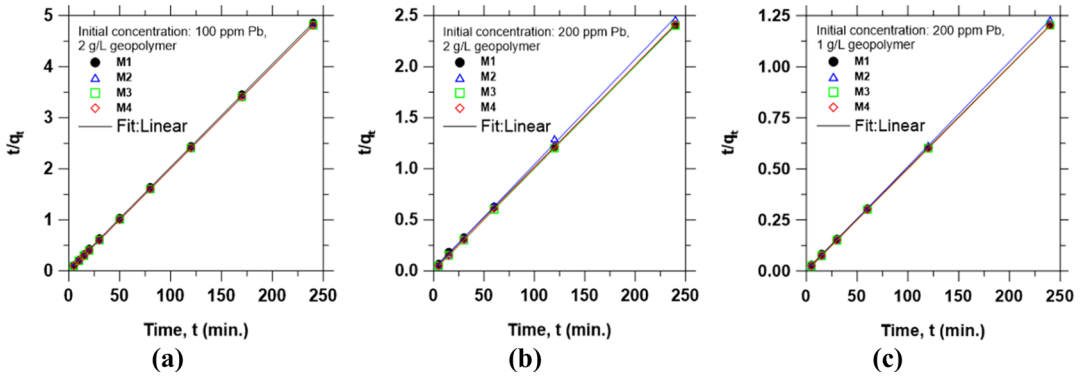

Figure 5. Pseudo-second-order kinetic model fitting of the sorption data for the three batch-sorption setups (a–c), with various initial Pb concentrations and geopolymer dosages.

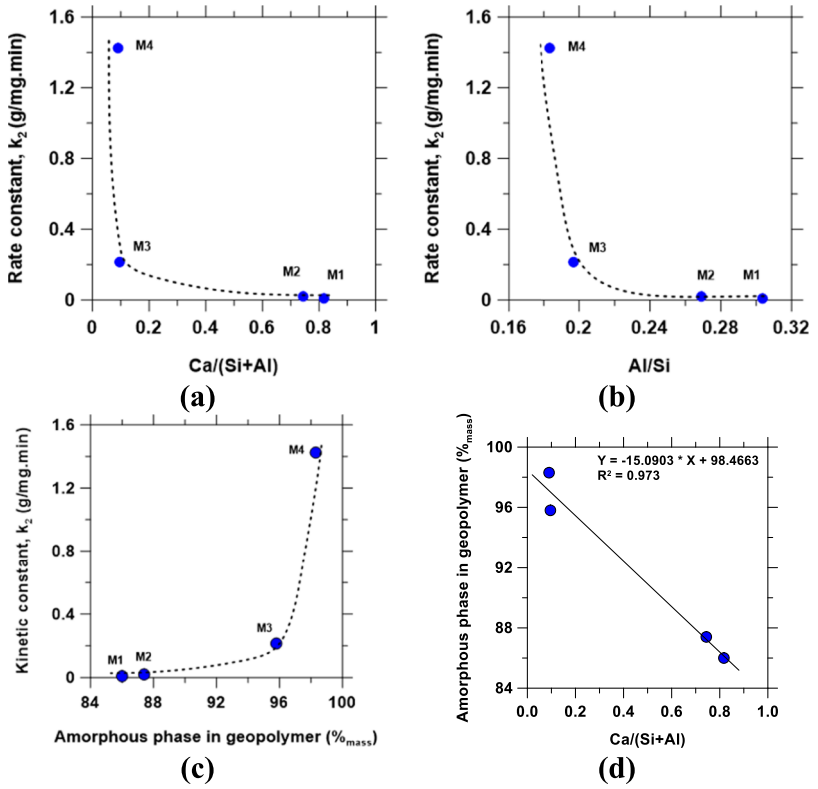

Figure 6. Evolution of the Pb sorption rate constant as a function of (a) Ca/(Si + Al), (b) Al/Si, (c) the percent amorphous phase of geopolymers, and (d) the percent amorphous phase as a function of Ca/(Si + Al). Dotted lines are "visual guides".

(i.e., M1 and M2) show more crystalline morphologies compared to the geopolymers prepared with Na_2SiO_3 (M3 and M4) which feature more amorphous phases, in agreement with the XRD patterns in Figure 1. The effects of the observed microstructural differences of the geopolymers on the Pb sorption kinetics and efficiency are examined in subsequent sections.

Figure 3 shows the particle size distribution and zeta potential of the geopolymer samples. The average particle size of pulverized geopolymer samples M1, M2, M3, and M4 were 0.733 μm, 2.267 μm, 1.813 μm, and 0.923 μm, respectively (corresponding to estimated specific surface areas SSAs of 1244.63, 854.16, 1390.43, and 2463.64 cm^2/g, respectively, calculated using the measured material densities and assuming that the particles are spherical). The measured zeta potential ranges from −28 to −34 mV (Figure 3b), in agreement with previous studies.[42,43] The considerable negative surface charge of the geopolymers is expected to encourage Pb sorption via an enhanced electrostatic interaction of the adsorbent surfaces and the positively charged aqueous Pb ion (i.e., Pb^{2+}).[44−47] The effect of particle surface and charge properties are examined in a later section (Section 2.4).

2.2. Effects of Composition and Microstructure on the Pb Sorption Kinetics. The kinetics of Pb sorption on the four different geopolymers (M1, M2, M3, and M4) were studied. Figure 4 shows the uptake of Pb as a function of contact time for the three different sorption setups. The results show that although the maximum Pb uptake per gram of the geopolymer is directly proportional to the initial concentration (Figure 4d), the kinetics of the sorption process is more complex and clearly dependent on the geopolymer composition (Figure 4a–c). The sorption kinetics lagged with M1, while in most cases of M3 and

https://dx.doi.org/10.1021/acsomega.0c02591
ACS Omega XXXX, XXX, XXX−XXX

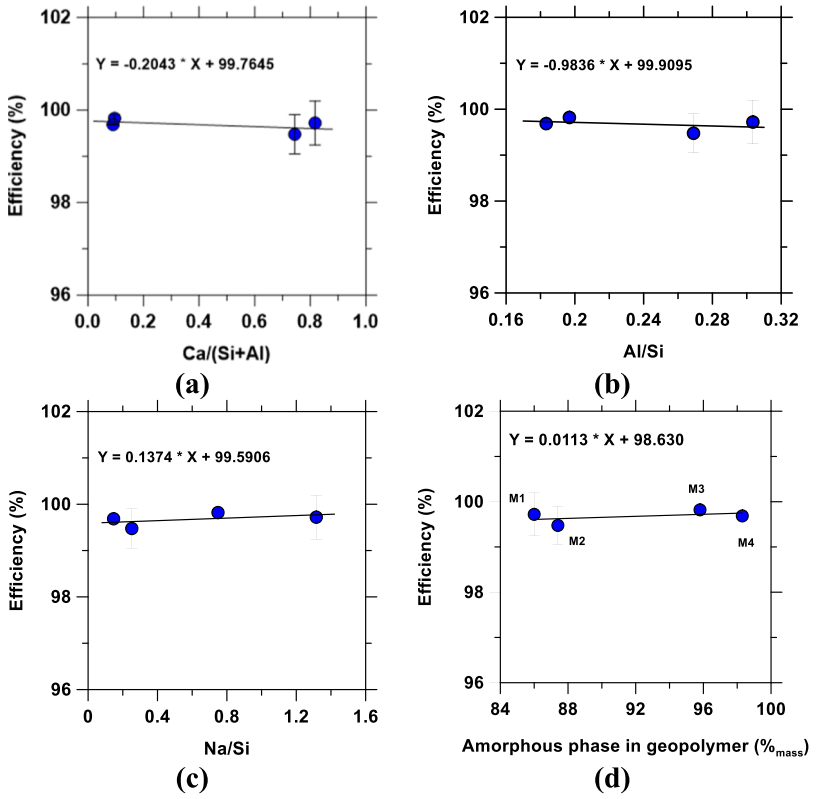

Figure 7. Evolution of Pb sorption efficiency as a function of (a) Ca/(Si + Al), (b) Al/Si, (c) Na/Si, and (d) the percent amorphous phase of the geopolymers.

M4, about 99.45% of Pb in solution had been removed within the first 5 min of sorption. However, the uptake of Pb in M1 gradually catches up with time, wherein the optimum removal efficiencies of all four geopolymers studied, M1 to M4, were 99.5% and above, which in comparison with previous studies is excellent.[25,48,49] For example, Al-Zboon et al.[29] obtained a 90.66% maximum Pb removal efficiency with the geopolymer prepared with Class F fly ash and 14 M NaOH activating solution, a comparable geopolymer formulation to the M2 of the present study. Also, Liu et al.[16] employed a mixture of NaOH and a sodium silicate activator with Class F fly ash and obtained a maximum Pb removal efficiency of 98.4% (at a sorption capacity of 24.6 mg/g) using 100 mg/L initial Pb concentration and a geopolymer dosage of 0.1 g/25 mL. More extensive review of the metal sorption performance of geopolymers prepared with different precursors and various formulation protocols have been presented elsewhere.[25,50]

In order to estimate the sorption rate, the sorption data were fitted with Lagergren's pseudo-first-order and pseudo-second-order kinetic models using eqs 1 and 2, respectively.[28,51,52]

$$\text{First order: } \ln(q_e - q_t) = \ln q_e - k_1 t \quad (1)$$

$$\text{Second order: } \frac{t}{q_t} = \frac{1}{k_2 q_e^2} + \frac{1}{q_e} t \quad (2)$$

where uptake q_t is the amount of Pb uptake by the geopolymer at a time t and q_e is the uptake at equilibrium. The sorption data fitted nicely to the pseudo-second-order model, with the correlation coefficients, $R^2 \geq 0.999$, in all the cases in this study (Figure 5) but did not fit very well with the pseudo-first-order model. As the sorption processes follow the second-order kinetics accurately, the rate-limiting step is thought to be chemisorption,[53−55] but the mechanism of the sorption process is discussed in more detail in Section 2.5.

To understand the effect of geopolymer composition and microstructure on the Pb sorption kinetics, the second-order rate constant, k_2, calculated from the model fitting, was examined as a function of the geopolymers' composition and microstructure (in terms of the percent amorphous phase distribution in the geopolymers' reaction product phase assemblage). Figure 6 shows that the rate constant decays exponentially with increasing Ca/(Si + Al) and Al/Si atomic ratios in the geopolymer composition and increases exponentially with increasing percent content of amorphous phases in the geopolymers' microstructure. The trend is consistent with the suggestion that high silica content (e.g., in M4) promotes the formation of the high-surface-area amorphous geopolymer (Figures 1 and 2 and Tables 1 and 3) which enhances the sorption kinetics through the increased number of accessible sorption sites. As seen in Figure 6d, the percentage of the amorphous phase content in the geopolymers decreases linearly with increasing Ca/(Si + Al) (also with increasing Ca/Si: not shown). This suggests that for low silica fly ash (e.g., high Ca fly ash precursors), the performance can be improved using silicate activators, as seen in the case of M3 which involved the same precursor used for M1 but activated with a sodium silicate solution.

2.3. Effect of Geopolymer Composition and Microstructure on the Pb Sorption Efficiency. Both the composition and microstructure of geopolymers have significant impacts on the physicochemical properties of the materials,[56] including the heavy metal sorption kinetics (as seen in the preceding section) and the sorption efficiency. In this section, the Pb removal efficiency was examined as a function of the

https://dx.doi.org/10.1021/acsomega.0c02591
ACS Omega XXXX, XXX, XXX−XXX

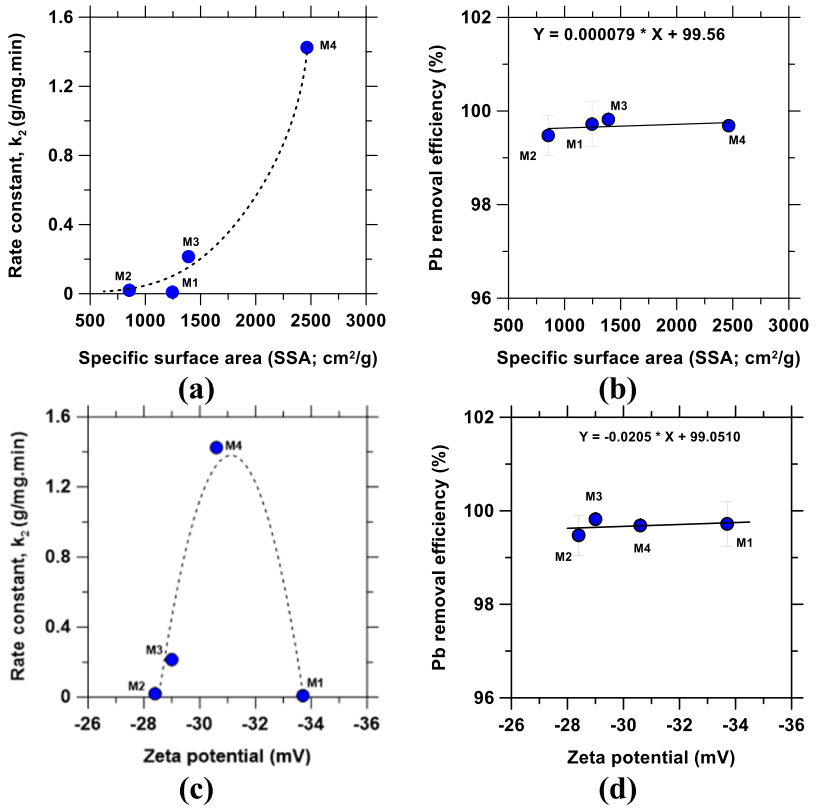

Figure 8. (a,b) Sorption rate constant and Pb removal efficiency as a function of specific surface area; (c,d) sorption rate constant and Pb removal efficiency as a function of zeta potential of the geopolymer particles. Dotted lines are "visual guides".

composition and microstructural parameters of the synthesized geopolymers. The average of the Pb removal efficiency, calculated using eq 5, for the different batch sorption experiments was investigated. Figure 7 shows the evolution of efficiency with respect to geopolymer compositions and microstructures. As seen in Figure 7a−d, the efficiency decreases slightly with increasing Ca/(Si + Al) and Al/Si but increases with increasing Na/Si and the mass percent of the amorphous content of the geopolymers' phase assemblage. These trends, similar but less strong compared to the impacts on the kinetics, again show that siliceous composition—which enhances the formation of high-surface-area three-dimensional geopolymer gel—is vital for enhanced Pb sorption performance.[57,58] Also, high Na content is expected to enhance the formation of the three-dimensional geopolymer gel,[59] and on the account of the high exchangeability of Na, thought to also improve the ion-exchange properties of the resulting geopolymer sorbent.

Although the geopolymers with high Ca−Al contents display lower kinetics (Figure 6), they do eventually catch up with the equilibrium Pb uptake amount that is comparable to the uptake obtained with the high Si counterparts (Figure 7). Thus, the impact of composition and microstructure is much more significant on the kinetics than the equilibrium uptake performance of the geopolymers. These findings are very crucial for informing the design of geopolymer sorbents for specific water treatment purposes. For example, in wastewater treatment where the resident time could be in the upward of an hour, either a high Ca−Al or a high Si geopolymer would be suitable, but for water filter applications where the resident time is often in the range of seconds to minutes, the use of the high Si geopolymer sorbent would be the most appropriate.

2.4. Effect of Particle Size and Surface Charge. The effect of particle size (or specific surface area, SSA) on the performance of adsorbents is well established in the literature, wherein smaller particle size provides higher specific surface area and active site density available for interaction with the absorbate, leading to enhanced sorption performance.[60,61] Expectedly, the Pb sorption kinetics and efficiency in the current study increases with increasing specific surface area of the geopolymer (Figure 8a,b), but at a lesser extent compared to the effects of composition and microstructure. The slope of the graph of efficiency versus SSA is 0.000079 (Figure 8b), a less significant number compared to the slopes of efficiency versus composition [i.e., Ca/(Si + Al): −0.2043, Al/Si: −0.9836, and Na/Si: 0.1374 (Figure 7a−c)] and efficiency versus microstructure [i.e., % amorphous phase: 0.0113 (Figure 7d)]. Similarly, to decouple the effects of composition and microstructure from possible effects of the small differences observed in zeta potential of the geopolymers (Figure 8c), the impacts of the zeta potential difference were examined. Sorption is expected to increase with increasing negative zeta potential[44] as a result of an increase in buoyancy and electrostatic interaction of the negatively charged geopolymer surface with the positively charged aqueous Pb(II) ions.[42−47] However, as shown in Figure 8c, the rate constant increased and then decreased with increasing negative zeta potential, contrary to the expected trend. Also, the Pb removal efficiency varies less significantly with zeta potentials of the four geopolymers (Figure 8d). This is partly due to the close values of the zeta potentials of M1 to M4, which are within −31 ± 3 mV. Thus, geopolymer M1 features the highest zeta potential value, yet displays the lowest sorption kinetics (Figure 8) compared to geopolymers M3 and M4, which further supports the dominating effect of

https://dx.doi.org/10.1021/acsomega.0c02591
ACS Omega XXXX, XXX, XXX−XXX

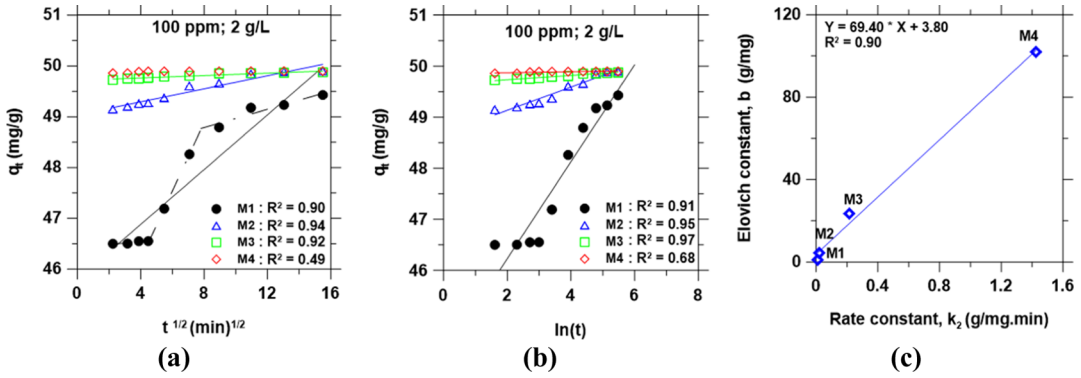

Figure 9. (a) IPD model fitting, (b) Elovich model fitting, and (c) the relationship between the Elovich constant b and the pseudo-second-order rate constant k_2.

composition and microstructure in controlling the sorption properties of the geopolymers in this study.

2.5. Sorption Mechanism. As seen in Figure 5, the Pb sorption processes fit excellently to the pseudo-second-order rate model, suggesting a chemisorption-controlled sorption.[62] To investigate the sorption process further, the data were tested with the intraparticle diffusion (IPD) model shown in eq 3.[63−66] From the transport phenomenon perspective, the Pb sorption process can be controlled by one or a combination of (i) the bulk solution transport, where the Pb diffuses from solution to the boundary layer of solution surrounding the geopolymer particles, (ii) film diffusion, where Pb diffuses through the liquid film surrounding the geopolymer particles; and(iii) pore diffusion and adsorption, where Pb is transported to the pores of the geopolymers to the available adsorption sites.[67]

$$\text{Intra-particle diffusion (IPD): } q_t = k_{id} \cdot t^{1/2} + \theta \quad (3)$$

where k_{id} is the IPD rate constant (mg/(g min$^{1/2}$)) and θ (mg/g) is a constant related to the thickness of the boundary layer; the larger the value of θ, the higher would be the boundary layer effect.[65,68] The sorption is diffusion-controlled if the graph of q_t versus $t^{1/2}$ is linear, indicating a sorption rate that is dependent on the rate at which the Pb and the geopolymer particles diffuse toward each other. Figure 9a shows that the data fit fairly to the IPD model which suggests that diffusion plays an important role, but in some cases, there is an obvious multilinear feature (e.g., M1), indicating that sorption is rather influenced by multiple processes.[65]

The sorption data were also examined with simplified Elovich's equation which has been extensively applied to describe chemisorption processes[69−76] (eq 4).

$$\text{Elovich's equation: } q_t = \frac{1}{b}\ln(ab) + \frac{1}{b}\ln(t) \quad (4)$$

where a is the initial adsorption rate (mg/(g min)) and the parameter b (g/mg) is often referred to as the desorption constant and has been thought to be related to the extent of surface coverage and activation energy of chemisorption;[72] if this equation applies, the graph of q_t versus ln(t) would yield a straight line. As shown in Figure 9b, the data produced a moderate fit to Elovich's equation, where a low coefficient of determination is obtained in some cases (e.g., M4) and a multilinear feature is observed in others (e.g., M1). Although the physical meaning of the b constant of the Elovich equation is not well understood, it can be assumed to be related to the number of available sorption sites.[77] As seen in Figure 9c, the pseudo-second-order rate constant is directly proportional to the b constant of the Elovich equation, suggesting that the sorption rate increases with increasing amount of available sorption sites in the geopolymer. In summary, all the abovementioned considerations suggest that Pb sorption by the geopolymers is controlled by a combination of chemisorption and particle diffusion. However, owing to the heterogeneous nature of the geopolymers, the overall physicochemical interaction appears to involve concurrent processes including surface adsorption, precipitation, ion exchange, chemisorption, and IPD. More specifically, (i) the high pH of the geopolymer systems encourages precipitation of Pb as insoluble Pb silicates in the pores of the geopolymer particles, leading to Pb removal from the aqueous solution,[36,78,79] (ii) Pb is also removed from the aqueous solution through ion exchange of Na^+ by Pb^{2+} in the charge balancing sites of the geopolymer framework,[80,81] and (iii) isovalent cationic substitution of Pb for other cations in relevant cementitious phases, for example, minor zeolites and C−S−H phases, and the formation of complexation products may occur in the system.[82] Thus, a combination of these multiple processes leads to the high Pb removal efficiency of the geopolymers.

The data were also applied to the Langmuir adsorption isotherm model,[83−88] which assumes the surface of the adsorbent as homogeneous and the energy of adsorption as equal for all sites,[87,89] and to the Freundlich adsorption isotherm model,[83,84,90,91] which assumes a heterogeneous adsorption surface with variation in the heat of adsorption.[29,92,93] These models did not produce a good fit for the sorption data in this study, which is thought to be because of the limited data points. However, this aspect is well studied in the literature where it had been suggested that Pb sorption follows these models, with better fitting reported for the Langmuir model than the Freundlich model in describing the adsorption of Pb on fly ash-based geopolymers.[16,29]

3. CONCLUSIONS

Fly ash-based geopolymers are a potential sustainable solution for the increasing demand for eco- and cost-efficient adsorbents for aqueous heavy metal removal. Geopolymers of different compositions and microstructures were prepared and studied for Pb removal. All the geopolymer materials studied displayed a Pb removal efficiency of 99.5% and above, an outstanding performance in the adsorption industry. However, it was shown that composition and microstructure greatly affect the sorption kinetics, with Pb sorption kinetics decreasing exponentially with

https://dx.doi.org/10.1021/acsomega.0c02591
ACS Omega XXXX, XXX, XXX−XXX

Table 2. Chemical Composition of Precursor Fly Ashes Used ($\%_{mass}$)

species	Na_2O	MgO	Al_2O_3	SiO_2	P_2O_5	SO_3	Cl	K_2O	CaO	TiO_2	Cr_2O_3	Mn_2O_3	Fe_2O_3	ZnO	SrO
FA-C[a]	0.95	5.28	16.82	32.67	1.47	1.76	0.05	0.54	32.48	1.41	0.01	0.034	6.13	0.02	0.38
FA-F[a]	0.64	1.53	19.04	57.00	0.74	1.22	0.08	2.47	6.10	0.76	0.04	0.049	10.21	0.08	0.03

[a]FA-C = class C fly ash; FA-F = class F fly ash.

Table 3. Composition Parameters of the Geopolymer Formulations (Elemental Ratios)

geopolymer	fly ash type	activator type	Ca/Si	Al/Si	Na/Si	Ca/(Si + Al)	(Na + Ca)/(Si + Al)
M1	FA-C	NaOH	1.065	0.303	1.315	0.817	1.826
M2	FA-F	NaOH	0.114	0.196	0.748	0.095	0.721
M3	FA-C	Na_2SiO_3	0.944	0.269	0.251	0.743	0.942
M4	FA-F	Na_2SiO_3	0.106	0.183	0.146	0.090	0.214

increasing Ca/(Si + Al) and Al/Si of the geopolymer composition but increases with increasing percentage of the amorphous phase in the microstructure of the geopolymers. The sorption efficiency was also found to show dependency on the composition and microstructure, but to a lesser extent compared to the dependency of sorption kinetics, wherein the Pb removal efficiency decreases slightly with increasing Ca/(Si + Al) and Al/Si of the geopolymer composition but increases with percent amorphous phases in the microstructure. In summary, high silica content, which enhances the formation of amorphous geopolymer phases, is found to be beneficial for high performance of the material in removing Pb from solution, while high Ca and Al favor the formation of more crystalline phases which greatly retard the sorption process. The 10 M NaOH-activated materials which, comparatively, are "more activated" featuring a high degree of fly ash reaction evidenced by the high crystalline morphology, compared to the sodium silicate-activated materials, appeared not to be the best solution. Conversely, the results indicate that the less-activated precursor (i.e., the Na_2SiO_3-activated) fly ashes produced better Pb adsorbents. Thus, the outcome of this research indicates that using appropriate precursor formulation and curing conditions to evoke the best microstructures, geopolymer materials can be optimized for high performance in removing heavy metals from wastewater.

Narrow temperature and pH conditions previously reported in the optimal range were used in this research. Further studies are therefore required to fully investigate the effects of variations of these parameters and others, including metal concentration per geopolymer dosage, multiple ion effects, selectivity, and the sorption reversibility. The waste geopolymers after Pb adsorption can be landfilled with a proper stabilization/solidification approach. However, the reusability of the material, in particular, is a subject of the subsequent project.

4. EXPERIMENTAL PROGRAM

4.1. Geopolymer Preparation. Two different fly ash precursors—ASTM-C618 type C fly ash (FA-C) and type F fly ash (FA-F) received from LafargeHolcim USA—were used to synthesize the geopolymers in this study. The composition of the fly ash precursors analyzed by X-ray fluorescence (XRF) spectroscopy is shown in Table 2. The fly ash precursors were reacted with both 10 M NaOH solution and 1 M Na_2SiO_3 solution (silica modulus: SiO_2/Na_2O = 1) prepared from reagent-grade chemicals to produce four geopolymers with different bulk compositions and microstructures. It is noted that a variety of alkaline activating solutions can be used to prepare geopolymers, but only sodium-based alkaline solutions are used in this study to keep the activator parameters simple, while investigating the impacts of composition and microstructure on the performance. Also, although the 10 M NaOH solution chosen in this study is known to sufficiently activate fly ash to produce the geopolymer,[40] the Na_2SiO_3 solution used singly is uncommon in the literature, but it yielded a beneficial high amorphous adsorbent, as discussed in Section 2. The molar ratio of major elements in each of the geopolymers is represented in Table 3. The fly ashes were mixed with the activating alkaline solutions at a solution/solid mass ratio of 0.7, under stirring at 850 rpm under ambient conditions for 20 min. The resulting pastes were cured in an oven at 90 °C for 24 h, followed by aging for 7 days at room temperature, in sealed plastic cubes. After aging, the synthesized geopolymers (M1, M2, M3, and M4; Table 1 and 3) were pulverized with a mortar and pestle and characterized by X-ray powder diffraction and SEM. The crystalline phases were identified utilizing the International Centre for Diffraction Data (ICDD) powder diffraction file database.

4.2. Sorption Tests. Batch sorption tests were conducted using 100 ppm and 200 ppm Pb solutions prepared from reagent grade lead(II) nitrate ($Pb(NO_3)_2$, Alfa Aesar) and deionized water (18.2 MΩ cm). For the 100 ppm system, a geopolymer dosage of 2 g/L was used, while for the 200 ppm solution, geopolymer dosages of 1 and 2 g/L were studied. For the three experimental setups, the sorption of Pb by the different geopolymers was monitored as a function of contact time from 5 to 240 min and by analysis of the filtered aliquot sample taken from the batch experiment at regular intervals. The sorption tests were conducted at 40 ± 0.5 °C[28] and at pH 7 ± 1 (adjusted with drops of NaOH solution), which lie within the conditions reported as optimal,[28,29,94] while the system was stirred continually at 300 rpm. The aliquot samples collected at time intervals were filtered with a 0.2 μm PTFE syringe filter, prior to dilution, acidification with 3% nitric acid, and elemental analysis by inductively coupled plasma optical emission spectrometry (ICP-OES). The Pb removal efficiency (%) was calculated using eq 5[29,94]

$$\text{removal efficiency (\%)} = \frac{C_0 - C_{eq}}{C_0} \times 100 \quad (5)$$

where C_0 is the initial concentration of Pb (ppm) and C_{eq} is the equilibrium concentration (ppm) of Pb in sorption solution. The Pb uptake by geopolymers was calculated according to the expression in eq 6[44,52,94−96]

$$q_t = \frac{(C_0 - C_{eq}) \times V}{W} \quad (6)$$

https://dx.doi.org/10.1021/acsomega.0c02591
ACS Omega XXXX, XXX, XXX−XXX

where uptake q_t (mg Pb/g of the geopolymer) is the amount of Pb uptake by the geopolymer at a time t, V is the volume of sorption solution (L), and W is the weight of the adsorbent (g).

4.3. Analytical Methods. For material characterization, several techniques were used. The oxide composition of fly ash was determined by XRF spectroscopy (Oxford X-Supreme 8000). The mineral phase assemblage in powdered fly ash precursors and synthesized geopolymers were examined by XRD using a PANalytical X'Pert Pro multipurpose diffractometer with a 2θ configuration using CuKα (λ = 1.540 Å) radiation and a fixed divergence and anti-scatter slit sizes of 0.5° and 0.25°, respectively. The X-ray generator was operated at a voltage of 45 kV and current of 40 mA. The pulverized samples were placed on the sample holder, surface-textured to minimize the preferred orientation, and scanned from 5 to 90° 2θ in a continuous manner at an integrated step size of 0.026° 2θ. For quantitative XRD analyses of geopolymers, the X'Pert High-Score Plus Rietveld method was used with corundum (Al_2O_3 anhydrous, $10\%_{mass}$) as the internal standard. The morphology of the fly ash and geopolymer samples was visualized using a scanning electron microscope (Hitachi S4700). A voltage of 20 kV was applied across the tungsten filament electron gun. A thin layer of finely ground selected samples was collected on a carbon-taped brass sample holder and gold-coated to prevent charging or overheating during the SEM analysis. The particle size analysis was accomplished utilizing a dynamic light scattering method with a Litesizer 500 by Anton Paar. Isopropanol was used as the dispersion media in this measurement, considering it will not react with the fly ash and geopolymer samples.[97,98] The solute to solvent ratio was maintained at 0.0006 g/mL. The specific surface areas of the geopolymer and fly ash samples were estimated using the density values measured with an Ultrapyc 1200e pycnometer. To know the surface charge values of the samples, zeta potential of the geopolymer particles dispersed in deionized water was also measured using the Litesizer 500.

For aqueous Pb concentration measurement, ICP-OES (AVIO 200 by PerkinElmer) was performed. Argon of ultrahigh purity (99.999%) was used to purge the optics and for plasma generation. The setup parameters used are as follows: 1500 W radio frequency power, 10 L min^{-1} plasma flow rate, 0.2 L min^{-1} auxiliary gas flow rate, 0.7 L min^{-1} nebulization gas flow rate, and a viewing distance of 15 mm. The solutions were introduced into the plasma using a concentric glass nebulizer (Meinhard, Golden CO, USA) with the aid of a peristaltic pump and an S10 autosampler (PerkinElmer) at a sample flow rate of 2.0 mL min^{-1}. The spectral line (wavelength) of the elemental Pb, 220.353 nm, was measured. The mean of triplicate measurements of the aqueous elemental speciation was used in the quantification of Pb remaining in the solution after each contact time of the sorption experiment. The detection limit for this ICP-OES is 0.1−100 ppm.

AUTHOR INFORMATION

Corresponding Author

Monday U. Okoronkwo − *Sustainable Materials Laboratory (SusMatLab), Department of Chemical and Biochemical Engineering and Department of Chemical and Biochemical Engineering, Missouri University of Science and Technology, Rolla, Missouri 65409, United States;* orcid.org/0000-0001-5033-9860; Phone: 573-341-4349; Email: okoronkwom@mst.edu

Authors

Sukanta K. Mondal − *Sustainable Materials Laboratory (SusMatLab), Department of Chemical and Biochemical Engineering, Missouri University of Science and Technology, Rolla, Missouri 65409, United States;* orcid.org/0000-0002-1880-1127

Adam Welz − *Sustainable Materials Laboratory (SusMatLab), Department of Chemical and Biochemical Engineering, Missouri University of Science and Technology, Rolla, Missouri 65409, United States*

Fateme Rezaei − *Department of Chemical and Biochemical Engineering, Missouri University of Science and Technology, Rolla, Missouri 65409, United States;* orcid.org/0000-0002-4214-4235

Aditya Kumar − *Department of Materials Science and Engineering, Missouri University of Science and Technology, Rolla, Missouri 65409, United States;* orcid.org/0000-0001-7550-8034

Complete contact information is available at: https://pubs.acs.org/10.1021/acsomega.0c02591

Notes

The authors declare no competing financial interest.

ACKNOWLEDGMENTS

Funding for this study was provided by the National Science Foundation (CMMI: 1932690) and the Materials Research Center (MRC) Young Investigators Seed Funding at Missouri S&T. The experiments were conducted at the Sustainable Materials Laboratory (SusMatLab), Materials Research Center (MRC), and the Center for Research in Energy and Environment (CREE), all at Missouri S&T. The authors would like to thank LafargeHolcim, Boral Resources, and Headwaters for the supply of fly ash samples.

REFERENCES

(1) Bolisetty, S.; Peydayesh, M.; Mezzenga, R. Sustainable technologies for water purification from heavy metals: review and analysis. *Chem. Soc. Rev.* **2019**, *48*, 463−487.

(2) Fu, F.; Wang, Q. Removal of heavy metal ions from wastewaters: a review. *J. Environ. Manage.* **2011**, *92*, 407−418.

(3) United Nations World Water Assessment Programme. *The world water development report 1: Water for people, water for life*; UNESCO: Paris, France, 2003.

(4) Pandey, P. K.; Sharma, S. K.; Sambi, S. S. Removal of lead (II) from waste water on zeolite-NaX. *J. Environ. Chem. Eng.* **2015**, *3*, 2604−2610.

(5) Barbosa, R.; Lapa, N.; Lopes, H.; Günther, A.; Dias, D.; Mendes, B. Biomass fly ashes as low-cost chemical agents for Pb removal from synthetic and industrial wastewaters. *J. Colloid Interface Sci.* **2014**, *424*, 27−36.

(6) Jamil, T. S.; Ibrahim, H. S.; Abd El-Maksoud, I. H.; El-Wakeel, S. T. Application of zeolite prepared from Egyptian kaolin for removal of heavy metals: I. Optimum conditions. *Desalination* **2010**, *258*, 34−40.

(7) Donat, R.; Akdogan, A.; Erdem, E.; Cetisli, H. Thermodynamics of Pb2+ and Ni2+ adsorption onto natural bentonite from aqueous solutions. *J. Colloid Interface Sci.* **2005**, *286*, 43−52.

(8) Assi, M. A.; Hezmee, M. N. M.; Haron, A. W.; Sabri, M. Y.; Rajion, M. A. The detrimental effects of lead on human and animal health. *Vet. World* **2016**, *9*, 660.

(9) Renfrew, D. Lead Poisoning and the Dangers of Pragmatism. *Int. J. Environ. Res. Publ. Health* **2018**, *15*, 1997.

(10) Raymond, J.; Brown, M. J. Childhood blood lead levels in children aged< 5 years—United States, 2009−2014. *MMWR Surveill. Summ.* **2017**, *66*, 1.

https://dx.doi.org/10.1021/acsomega.0c02591
ACS Omega XXXX, XXX, XXX−XXX

(11) Gupta, V. K.; Ali, I.; Saleh, T. A.; Nayak, A.; Agarwal, S. Chemical treatment technologies for waste-water recycling—an overview. *RSC Adv.* **2012**, *2*, 6380−6388.
(12) Kumar, P. S.; Saravanan, A. Sustainable Waste Water Treatment Technologies. *Detox Fashion*; Springer, 2018; pp 1−25.
(13) Zoubeik, M.; Ismail, M.; Salama, A.; Henni, A. New developments in membrane technologies used in the treatment of produced water: A review. *Arabian J. Sci. Eng.* **2018**, *43*, 2093−2118.
(14) Maruyama, T.; Hannah, S. A.; Cohen, J. M. Metal removal by physical and chemical treatment processes. *J. Water Pollut. Control Fed.* **1975**, *43*, 962−975.
(15) Barakat, M. A. New trends in removing heavy metals from industrial wastewater. *Arabian J. Chem.* **2011**, *4*, 361−377.
(16) Liu, Y.; Yan, C.; Zhang, Z.; Wang, H.; Zhou, S.; Zhou, W. A comparative study on fly ash, geopolymer and faujasite block for Pb removal from aqueous solution. *Fuel* **2016**, *185*, 181−189.
(17) Erto, A.; Di Natale, F.; Musmarra, D.; Lancia, A. Modeling of single and competitive adsorption of cadmium and zinc onto activated carbon. *Adsorption* **2015**, *21*, 611−621.
(18) Bortone, I.; Di Nardo, A.; Di Natale, M.; Erto, A.; Musmarra, D.; Santonastaso, G. F. Remediation of an aquifer polluted with dissolved tetrachloroethylene by an array of wells filled with activated carbon. *J. Hazard. Mater.* **2013**, *260*, 914−920.
(19) Davidovits, J. Geopolymers. *J. Therm. Anal. Calorim.* **1991**, *37*, 1633−1656.
(20) Duxson, P.; Fernández-Jiménez, A.; Provis, J. L.; Lukey, G. C.; Palomo, A.; van Deventer, J. S. J. Geopolymer technology: the current state of the art. *J. Mater. Sci.* **2007**, *42*, 2917−2933.
(21) Wang, J.; Wu, X.-l.; Wang, J.-x.; Liu, C.-z.; Lai, Y.-m.; Hong, Z.-k.; Zheng, J.-p. Hydrothermal synthesis and characterization of alkali-activated slag−fly ash−metakaolin cementitious materials. *Microporous Mesoporous Mater.* **2012**, *155*, 186−191.
(22) Ahmaruzzaman, M. A review on the utilization of fly ash. *Prog. Energy Combust. Sci.* **2010**, *36*, 327−363.
(23) Li, L.; Wang, S.; Zhu, Z. Geopolymeric adsorbents from fly ash for dye removal from aqueous solution. *J. Colloid Interface Sci.* **2006**, *300*, 52−59.
(24) Álvarez-Ayuso, E.; Querol, X.; Plana, F.; Alastuey, A.; Moreno, N.; Izquierdo, M.; Font, O.; Moreno, T.; Diez, S.; Vázquez, E.; Barra, M. Environmental, physical and structural characterisation of geopolymer matrixes synthesised from coal (co-) combustion fly ashes. *J. Hazard. Mater.* **2008**, *154*, 175−183.
(25) Siyal, A. A.; Shamsuddin, M. R.; Khan, M. I.; Rabat, N. E.; Zulfiqar, M.; Man, Z.; Siame, J.; Azizli, K. A. A review on geopolymers as emerging materials for the adsorption of heavy metals and dyes. *J. Environ. Manage.* **2018**, *224*, 327−339.
(26) Harja, I. G. O. M.; Barbuta, M.; Gavrilescu, M. Utilization of Coal Fly Ash from Power Plants. *Environ. Eng. Manage. J.* **2009**, *8*, 513−520.
(27) Andini, S.; Cioffi, R.; Colangelo, F.; Grieco, T.; Montagnaro, F.; Santoro, L. Coal fly ash as raw material for the manufacture of geopolymer-based products. *Waste Manag.* **2008**, *28*, 416−423.
(28) Al-Harahsheh, M. S.; Al Zboon, K.; Al-Makhadmeh, L.; Hararah, M.; Mahasneh, M. Fly ash based geopolymer for heavy metal removal: A case study on copper removal. *J. Environ. Chem. Eng.* **2015**, *3*, 1669−1677.
(29) Al-Zboon, K.; Al-Harahsheh, M. S.; Hani, F. B. Fly ash-based geopolymer for Pb removal from aqueous solution. *J. Hazard. Mater.* **2011**, *188*, 414−421.
(30) Khale, D.; Chaudhary, R. Mechanism of geopolymerization and factors influencing its development: a review. *J. Mater. Sci.* **2007**, *42*, 729−746.
(31) Wang, S.; Li, L.; Zhu, Z. H. Solid-state conversion of fly ash to effective adsorbents for Cu removal from wastewater. *J. Hazard. Mater.* **2007**, *139*, 254−259.
(32) Zhang, Y.; Sun, W.; She, W.; Sun, G. Synthesis and heavy metal immobilization behaviors of fly ash based gepolymer. *J. Wuhan Univ. Technol., Mater. Sci. Ed.* **2009**, *24*, 819.
(33) Davidovits, J. Carbon-dioxide greenhouse-warming: what future for Portland cement. *Emerging Technologies Symposium on Cements and Concretes in the Global Environment*; Portland Cement Association: Chicago, Illinois, 1993; p 21.
(34) Yunsheng, Z.; Wei, S.; Qianli, C.; Lin, C. Synthesis and heavy metal immobilization behaviors of slag based geopolymer. *J. Hazard. Mater.* **2007**, *143*, 206−213.
(35) Fernandez-Jimenez, A.; Palomo, A. Chemical durability of geopolymers. *Geopolymers*; Elsevier, 2009; pp 167−193.
(36) Glasser, F. P. Fundamental aspects of cement solidification and stabilisation. *J. Hazard. Mater.* **1997**, *52*, 151−170.
(37) Guo, B.; Liu, B.; Yang, J.; Zhang, S. The mechanisms of heavy metal immobilization by cementitious material treatments and thermal treatments: A review. *J. Environ. Manage.* **2017**, *193*, 410−422.
(38) Okoronkwo, M. U.; Balonis, M.; Katz, L.; Juenger, M.; Sant, G. A thermodynamics-based approach for examining the suitability of cementitious formulations for solidifying and stabilizing coal-combustion wastes. *J. Environ. Manage.* **2018**, *217*, 278−287.
(39) Maleki, A.; Hajizadeh, Z.; Sharifi, V.; Emdadi, Z. A green, porous and eco-friendly magnetic geopolymer adsorbent for heavy metals removal from aqueous solutions. *J. Cleaner Prod.* **2019**, *215*, 1233−1245.
(40) Rattanasak, U.; Chindaprasirt, P. Influence of NaOH solution on the synthesis of fly ash geopolymer. *Miner. Eng.* **2009**, *22*, 1073−1078.
(41) Zhang, M.; El-Korchi, T.; Zhang, G.; Liang, J.; Tao, M. Synthesis factors affecting mechanical properties, microstructure, and chemical composition of red mud−fly ash based geopolymers. *Fuel* **2014**, *134*, 315−325.
(42) Gunasekara, C.; Law, D. W.; Setunge, S.; Sanjayan, J. G. Zeta potential, gel formation and compressive strength of low calcium fly ash geopolymers. *Constr. Build. Mater.* **2015**, *95*, 592−599.
(43) Alehyen, S.; Achouri, M.; Taibi, M. Characterization, microstructure and properties of fly ash-based geopolymer. *J. Mater. Environ. Sci.* **2017**, *8*, 1783−1796.
(44) He, C.; Xie, F. Adsorption behavior of manganese dioxide towards heavy metal ions: Surface Zeta potential effect. *Water, Air, Soil Pollut.* **2018**, *229*, 77.
(45) Sadowski, Z. Effect of biosorption of Pb(II), Cu(II) and Cd(II) on the zeta potential and flocculation of Nocardia sp. *Miner. Eng.* **2001**, *14*, 547−552.
(46) Erdemoğlu, M.; Sarikaya, M. Effects of heavy metals and oxalate on the zeta potential of magnetite. *J. Colloid Interface Sci.* **2006**, *300*, 795−804.
(47) Savaji, K. V.; Niitsoo, O.; Couzis, A. Influence of particle/solid surface zeta potential on particle adsorption kinetics. *J. Colloid Interface Sci.* **2014**, *431*, 165−175.
(48) Ariffin, N.; Abdullah, M. M. A. B.; Mohd Arif Zainol, M. R. R.; Murshed, M. F.; Hariz-Zain, M. A.; Faris, M. A.; Bayuaji, R. Review on adsorption of heavy metal in wastewater by using geopolymer. *MATEC Web Conf.* **2017**, *97*, 01023.
(49) Al-Zboon, K. K.; Al-smadi, B. M.; Al-Khawaldh, S. Natural volcanic tuff-based geopolymer for Zn removal: adsorption isotherm, kinetic, and thermodynamic study. *Water, Air, Soil Pollut.* **2016**, *227*, 248.
(50) Tan, T. H.; Mo, K. H.; Ling, T.-C.; Lai, S. H. Current development of geopolymer as alternative adsorbent for heavy metal removal. *Environ. Technol. Innov.* **2020**, *18*, 100684.
(51) Gupta, S. S.; Bhattacharyya, K. G. Kinetics of adsorption of metal ions on inorganic materials: a review. *Adv. Colloid Interface Sci.* **2011**, *162*, 39−58.
(52) Uddin, M. T.; Rahman, M. A.; Rukanuzzaman, M.; Islam, M. A. A potential low cost adsorbent for the removal of cationic dyes from aqueous solutions. *Appl. Water Sci.* **2017**, *7*, 2831−2842.
(53) Ho, Y. S.; McKay, G. Pseudo-second order model for sorption processes. *Process Biochem.* **1999**, *34*, 451−465.
(54) Ho, Y. Review of second-order models for adsorption systems. *J. Hazard. Mater.* **2006**, *136*, 681−689.
(55) Juang, R.-S.; Lin, S.-H.; Tsao, K.-H. Mechanism of sorption of phenols from aqueous solutions onto surfactant-modified montmorillonite. *J. Colloid Interface Sci.* **2002**, *254*, 234−241.

https://dx.doi.org/10.1021/acsomega.0c02591
ACS Omega XXXX, XXX, XXX−XXX

(56) Rakhimova, N. R.; Rakhimov, R. Z. Reaction products, structure and properties of alkali-activated metakaolin cements incorporated with supplementary materials − a review. *J. Mater. Res. Technol.* **2019**, *8*, 1522−1531.
(57) Zhang, Q.; Lin, B.; Hong, J.; Chang, C.-T. Removal of ammonium and heavy metals by cost-effective zeolite synthesized from waste quartz sand and calcium fluoride sludge. *Water Sci. Technol.* **2017**, *75*, 587−597.
(58) Nelson, J.; Wasylenki, L.; Bargar, J. R.; Brown, G. E.; Maher, K. Effects of surface structural disorder and surface coverage on isotopic fractionation during Zn(II) adsorption onto quartz and amorphous silica surfaces. *Geochim. Cosmochim. Acta* **2017**, *215*, 354−376.
(59) Davidovits, J. *Geopolymer Chemistry and Applications*, 5th ed.; Institut Géopolymère: Saint-Quentin, France, 2020.
(60) Tsai, W. T.; Lai, C. W.; Hsien, K. J. Effect of particle size of activated clay on the adsorption of paraquat from aqueous solution. *J. Colloid Interface Sci.* **2003**, *263*, 29−34.
(61) Wang, H.; Shadman, F. Effect of particle size on the adsorption and desorption properties of oxide nanoparticles. *AIChE J.* **2013**, *59*, 1502−1510.
(62) Robati, D. Pseudo-second-order kinetic equations for modeling adsorption systems for removal of lead ions using multi-walled carbon nanotube. *J. Nanostruct. Chem.* **2013**, *3*, 55.
(63) Weber, W. J.; Morris, J. C. Kinetics of adsorption on carbon from solution. *J. Sanit. Eng. Div.* **1963**, *89*, 31−60.
(64) Wu, F.-C.; Tseng, R.-L.; Juang, R.-S. Initial behavior of intraparticle diffusion model used in the description of adsorption kinetics. *Chem. Eng. J.* **2009**, *153*, 1−8.
(65) Fierro, V.; Torné-Fernández, V.; Montané, D.; Celzard, A. Adsorption of phenol onto activated carbons having different textural and surface properties. *Microporous Mesoporous Mater.* **2008**, *111*, 276−284.
(66) Simonin, J.-P.; Bouté, J. Intraparticle diffusion-adsorption model to describe liquid/solid adsorption kinetics. *Rev. Mex. Ing. Quim.* **2016**, *15*, 161−173.
(67) Singh, S. K.; Townsend, T. G.; Mazyck, D.; Boyer, T. H. Equilibrium and intra-particle diffusion of stabilized landfill leachate onto micro-and meso-porous activated carbon. *Water Res.* **2012**, *46*, 491−499.
(68) Kannan, N.; Sundaram, M. M. Kinetics and mechanism of removal of methylene blue by adsorption on various carbons—a comparative study. *Dyes Pigm.* **2001**, *51*, 25−40.
(69) Aharoni, C.; Tompkins, F. C. Kinetics of adsorption and desorption and the Elovich equation. *Adv. Catal.* **1970**, *21*, 1−49.
(70) Juang, R.-S.; Chen, M.-L. Application of the Elovich equation to the kinetics of metal sorption with solvent-impregnated resins. *Ind. Eng. Chem. Res.* **1997**, *36*, 813−820.
(71) Wu, F.-C.; Tseng, R.-L.; Juang, R.-S. Characteristics of Elovich equation used for the analysis of adsorption kinetics in dye-chitosan systems. *Chem. Eng. J.* **2009**, *150*, 366−373.
(72) Örnek, A.; Özacar, M.; Şengil, İ. A. Adsorption of lead onto formaldehyde or sulphuric acid treated acorn waste: equilibrium and kinetic studies. *Biochem. Eng. J.* **2007**, *37*, 192−200.
(73) Han, R.; Zou, W.; Zhang, Z.; Shi, J.; Yang, J. Removal of copper(II) and lead(II) from aqueous solution by manganese oxide coated sand. *J. Hazard. Mater.* **2006**, *137*, 384−395.
(74) Malkoc, E.; Nuhoglu, Y. Determination of kinetic and equilibrium parameters of the batch adsorption of Cr (VI) onto waste acorn of Quercus ithaburensis. *Chem. Eng. Process.* **2007**, *46*, 1020−1029.
(75) Ho, Y. S.; McKay, G. A comparison of chemisorption kinetic models applied to pollutant removal on various sorbents. *Process Saf. Environ. Protect.* **1998**, *76*, 332−340.
(76) Cheung, C. W.; Porter, J. F.; McKay, G. Sorption kinetic analysis for the removal of cadmium ions from effluents using bone char. *Water Res.* **2001**, *35*, 605−612.
(77) Riahi, K.; Chaabane, S.; Thayer, B. B. A kinetic modeling study of phosphate adsorption onto Phoenix dactylifera L. date palm fibers in batch mode. *J. Saudi Chem. Soc.* **2017**, *21*, S143−S152.
(78) Palomo, A.; Palacios, M. Alkali-activated cementitious materials: Alternative matrices for the immobilisation of hazardous wastes. *Cem. Concr. Res.* **2003**, *33*, 289−295.
(79) Palacios, M.; Palomo, A. Alkali-activated fly ash matrices for lead immobilisation: a comparison of different leaching tests. *Adv. Cem. Res.* **2004**, *16*, 137−144.
(80) Skorina, T. Ion exchange in amorphous alkali-activated aluminosilicates: potassium based geopolymers. *Appl. Clay Sci.* **2014**, *87*, 205−211.
(81) O'Connor, S. J.; MacKenzie, K. J. D.; Smith, M. E.; Hanna, J. V. Ion exchange in the charge-balancing sites of aluminosilicate inorganic polymers. *J. Mater. Chem.* **2010**, *20*, 10234−10240.
(82) Żak, R.; Deja, J. Spectroscopy study of Zn, Cd, Pb and Cr ions immobilization on C−S−H phase. *Spectrochim. Acta, Part A* **2015**, *134*, 614−620.
(83) LeVan, M. D.; Vermeulen, T. Binary Langmuir and Freundlich isotherms for ideal adsorbed solutions. *J. Phys. Chem.* **1981**, *85*, 3247−3250.
(84) Chung, H.-K.; Kim, W.-H.; Park, J.; Cho, J.; Jeong, T.-Y.; Park, P.-K. Application of Langmuir and Freundlich isotherms to predict adsorbate removal efficiency or required amount of adsorbent. *J. Ind. Eng. Chem.* **2015**, *28*, 241−246.
(85) Li, Q.; Zhai, J.; Zhang, W.; Wang, M.; Zhou, J. Kinetic studies of adsorption of Pb (II), Cr (III) and Cu (II) from aqueous solution by sawdust and modified peanut husk. *J. Hazard. Mater.* **2007**, *141*, 163−167.
(86) Soldatini, G. F.; Riffaldi, R.; Levi-Minzi, R. Pb adsorption by soils. *Water, Air, Soil Pollut.* **1976**, *6*, 111−118.
(87) Masel, R. I. *Principles of Adsorption and Reaction on Solid Surfaces*; John Wiley & Sons, 1996; Vol. *3*.
(88) Kleman, M.; Laverntovich, O. D. *Soft Matter Physics: An Introduction*; Springer Science & Business Media, 2007.
(89) Misra, A.; Gupta, R.; Gupta, R. Utilization of marble slurry in construction materials. *Workshop on Gainful Utilization of Marble Slurry and Other Stone Waste*; Indian School of Mines, accessed, 2008.
(90) Freundlich, H. Über die adsorption in lösungen. *Z. Phys. Chem.* **1907**, *57*, 385−470.
(91) Freundlich, H. *Kapillarchemie, eine Darstellung der Chemie der Kolloide und verwandter Gebiete*; Akademische Verlagsgesellschaft, 1922.
(92) Manohar, D. M.; Noeline, B. F.; Anirudhan, T. S. Adsorption performance of Al-pillared bentonite clay for the removal of cobalt (II) from aqueous phase. *Appl. Clay Sci.* **2006**, *31*, 194−206.
(93) Adamson, A. W.; Gast, A. P. *Physical Chemistry of Surfaces*; Interscience publishers: New York, 1967; Vol. *150*.
(94) He, K.; Chen, Y.; Tang, Z.; Hu, Y. Removal of heavy metal ions from aqueous solution by zeolite synthesized from fly ash. *Environ. Sci. Pollut. Res. Int.* **2016**, *23*, 2778−2788.
(95) Xu, D.; Tan, X.; Chen, C.; Wang, X. Adsorption of Pb (II) from aqueous solution to MX-80 bentonite: effect of pH, ionic strength, foreign ions and temperature. *Appl. Clay Sci.* **2008**, *41*, 37−46.
(96) Ge, Y.; Cui, X.; Kong, Y.; Li, Z.; He, Y.; Zhou, Q. Porous geopolymeric spheres for removal of Cu(II) from aqueous solution: synthesis and evaluation. *J. Hazard. Mater.* **2015**, *283*, 244−251.
(97) Zhang, J.; Scherer, G. W. Comparison of methods for arresting hydration of cement. *Cem. Concr. Res.* **2011**, *41*, 1024−1036.
(98) Ferraris, C. F.; Avilés, A. I.; Hackley, V. A. Measurement of Particle Size Distribution in Portland Cement Powder: Analysis of ASTM Round Robin Studies. *Cem., Concr., Aggregates* **2004**, *26*, 1−11.

https://dx.doi.org/10.1021/acsomega.0c02591
ACS Omega XXXX, XXX, XXX−XXX